Eye lens isotope tag reveal migration as a driver of Japanese sardine synchrony

Authors

Tatsuya Sakamoto^{1,2*}, Motomitsu Takahashi¹, Kotaro Shirai³, Satoshi Kitajima¹, Toyoho Ishimura⁴

- 1. Fisheries Resources Institute, Japan Fisheries Research and Education Agency, Nagasaki, Japan
- 2. The Hakubi Center for Advanced Research, Kyoto University, Kyoto, Japan
- 3. Atmosphere and Ocean Research Institute, The University of Tokyo, Chiba, Japan
- 4. Graduate School of Human and Environmental Studies, Kyoto University, Kyoto, Japan

*Corresponding author

Email: sakamoto.tatsuya.3p@kyoto-u.ac.jp

Present address: Yoshidanihonmatsucho, Kyoto Sakyo-ku, Kyoto, 606-8316 Japan

Abstract

Understanding population fluctuations of broadly distributed marine fishes remains difficult, partly because they often consist of cryptic mixtures of individuals originating from geographically distinct nurseries that experience different environment pressures. However, resolving these spatiotemporally changing mixing processes had been challenging as conventional techniques are highly resource- and time-consuming. Here, we present a high-throughput approach using archival stable isotopes (carbon and nitrogen) in fish eye lens centers as a reliable natural tag of nursery origin. Applied to > 2000 Japanese sardine in the western North Pacific, a species long assumed to comprise two distinct subpopulations, the age-0 isotope baselines showed clear and temporally consistent geographical variation, allowing robust classification of recruitment source. Analysis of adults collected between 2019 and 2023 revealed the recruits from the offshore Pacific were dominated not only the major fishing ground in the Pacific but also the spawning grounds in the Sea of Japan and East China Sea, directly contradicting the long-standing two-stock model. These trans-boundary migration of Pacific recruits explain the century-long synchrony observed between putative subpopulations, and alter the ecosystem structure at the destination. This scalable method is applicable across mobile marine fauna, providing a crucial tool for spatial ecosystem management under rapid climate change.

Introduction

Marine fisheries support the global food supply by providing a significant source of animal protein for direct human consumption¹, and by supplying fishmeal and fish oil that are essential inputs for aquaculture production². However, marine fish populations often fluctuate intensely³, and the mechanisms behind these fluctuations are notoriously difficult to understand. Various factors such as environmental variabilities⁴, fishing pressures⁵, population densities⁶ and species interactions, can affect fish growth and survival in nonlinear and nonstationary manners^{7,8}. A key challenge is that fish population often comprises groups from multiple spawning and nursery areas of different environmental conditions⁹, in which fish are subjected to differential pressures^{10,11}. Unawareness of such mixing substantially disrupts understanding the causes of population fluctuations, and also biases the estimates of abundances as the assessment models often assume that data is obtained from a population with limited im- and emigrations and uniform vital rates¹². Disentangling spatiotemporally varying mixing process in a population is therefore crucial for monitoring and understanding population dynamics, and ensuring sustainable fisheries through effective conservation schemes¹³.

Variable methods, such as archival tags¹⁴, genomics^{15,16}, hard structure chemistries (e.g., otoliths⁹) or combination of the chemistry and numerical simulation¹⁷, have successfully allowed robust identifications of fish origin and illustrated migration patterns in oceans. However, understanding the mixing process in a habitat-wide scale, together with its temporal variation, necessarily requires large empirical datasets including hundreds to thousands of samples^{9,18}. As the conventional methods require costly laboratory equipment, experienced technicians and heavy workloads, comprehensive assessments of mixing and connectivity remain an expensive and often impracticable task¹⁹. Molecular tools have advanced rapidly and are now widely used to assess population structure, although they predominantly capture evolutionary rather than ecological timescales¹², and thus provide limited insight into the changes occurring in contemporary populations under the rapid climate change.

Chemistry in eye lenses, the incrementally-growing protein structure in eye balls, is an emerging and promising solution. As the fibre cells of the lens layers i.e. laminae hardly

undergo turnovers after formation, their chemical compositions that reflect those of prey are likely preserved^{20,21}. The carbon and nitrogen isotope values (δ^{13} C and δ^{15} N) of marine organisms reflect trophic positions and isotope values of primary producer, phytoplankton, which significantly vary depending on temperature, species composition and nutrient source and availability²²⁻²⁵. Spatially varying isotope values can therefore be recorded in eye lenses, allowing inferences about localities²⁶⁻²⁹. Eye lens subsampling can be done with only forceps and a stereomicroscope, whereas conventional hard-structure analyses typically require processing using expensive microdrills or laser ablation systems after careful sectioning^{9,30}. As a result, the laboratory set-up costs and sample preparation time can be reduced by as much as an order of magnitude (see Supplementary Information). In addition, the analysis of bulk δ^{13} C and δ^{15} N of organic materials is well-established for food-web analysis and therefore reasonable, suggesting the significant potential of eye lens isotopes as a scalable natural tag. However, important validations, such as the intrabody offsets, validity as a recorder of prey isotopes, the extent of geographical variation and its robustness against temporal variabilities, remain sparce, leaving the reliability of eye lens isotopes for fisheries management unconfirmed.

Japanese sardine Sardinops sagax melanostictus is one of the largest small pelagic fish populations on earth, known for its intense population fluctuation³¹. The plankton feeder inhabits the western North Pacific and its marginal seas, namely the Sea of Japan and East China Sea (SJ-ECS), separated by the Japanese archipelago, narrow straits and strong current (Fig. 1a). The population had provided annual catch of over 5 million tons in the late 1980s before collapsing in the 1990s, and is increasing again since 2010s (Fig. 1b, c). As typical of small pelagic fish that plays the key role of transferring energy from plankton to upper trophic levels³², its population fluctuation has significantly impacted the zooplankton biomass in the region via top-down effect³³, and also the biomass and distribution of competitors³⁴ and predator^{35,36}. Decades have passed since the basin-scale decadal environmental variabilities were hypothesised as the primary driver^{3,37}. Cooler climate has been considered favourable for the sardine, hypothetically mediated by bottom-up effect^{38,39} or thermal response of early life growth⁴⁰ or combination of these¹⁰. However, the recent recovery has occurred under warmer conditions than the previous increasing periods⁴¹, highlighting gaps in our understanding of the physical drivers of sardine population dynamics.

The overlooked feature in Japanese sardine is the century-long, synchronised fluctuations in abundance in the Pacific and SJ-ECS (Fig. 1). Spawning occurs off the Japanese coast on both sides from winter to spring^{42,43} (Fig. 1a), with larvae and juveniles found near coastal spawning areas or offshore in the Pacific 10,44. Two semi-independent subpopulations, one in the Pacific and another in SJ-ECS, have long been assumed in stock assessment and fisheries managements⁴⁴⁻⁴⁷ and in most researches of population fluctuation^{5,8,10,48}. Different somatic growth rates in recent years, sharply slowing down in the Pacific and only a minor change in the SJ-ECS^{49,50}, are supportive of the separation. If this is indeed the case, a common physical driver could explain the synchronized fluctuations in the two areas. For example, as the Tsushima Warm Current in the SJ-ECS mainly originates from the intrusion of the Kuroshio to the continental shelf⁵¹, the environmental variabilities in the upstream Kuroshio might simultaneously influence nursery environments and survival in both regions. However, the synchrony could also result from fish mixing, a possibility poorly tested. Nakai⁵² hypothesised significant sardine migrations from Pacific to SJ-ECS based on cohort tracking, which has not been favoured in later researches given the narrow straits and opposing eastward current⁵³. Still, no geographical differentiation in the mitochondrial DNA was detected⁵⁴, and recent otolith isotope analysis also suggests that the main source of recruitment in the SJ-ECS can be Pacific origin³⁰. Clarifying the cause of this synchrony is crucial for understanding sardine population dynamics and reassessing stock assessment models, which underpin fisheries management and research.

In this study, we conducted δ^{13} C and δ^{15} N analyses of eye lens centres from more than 2000 individuals to investigate the habitat-wide mixing patterns of the Japanese sardine, which have remained unclear despite long-term field surveys. We first characterised the isotopic signatures of juveniles from known recruitment areas and built a classification model to allow inferences of nursery origin. We then applied this model to adults to reconstruct their movements. A series of validations using phytoplankton isoscapes, stable isotopes of muscles, and otoliths was performed to understand the mechanisms driving variation in eye lens isotopes and to test their robustness as a natural tag. Our results reveal significant migrations across the traditional management border and clarify the source-sink dynamics in the ecologically key species in the North Pacific ecosystem, thereby highlighting the effectiveness of eye lens analysis in improving understanding of marine population dynamics.

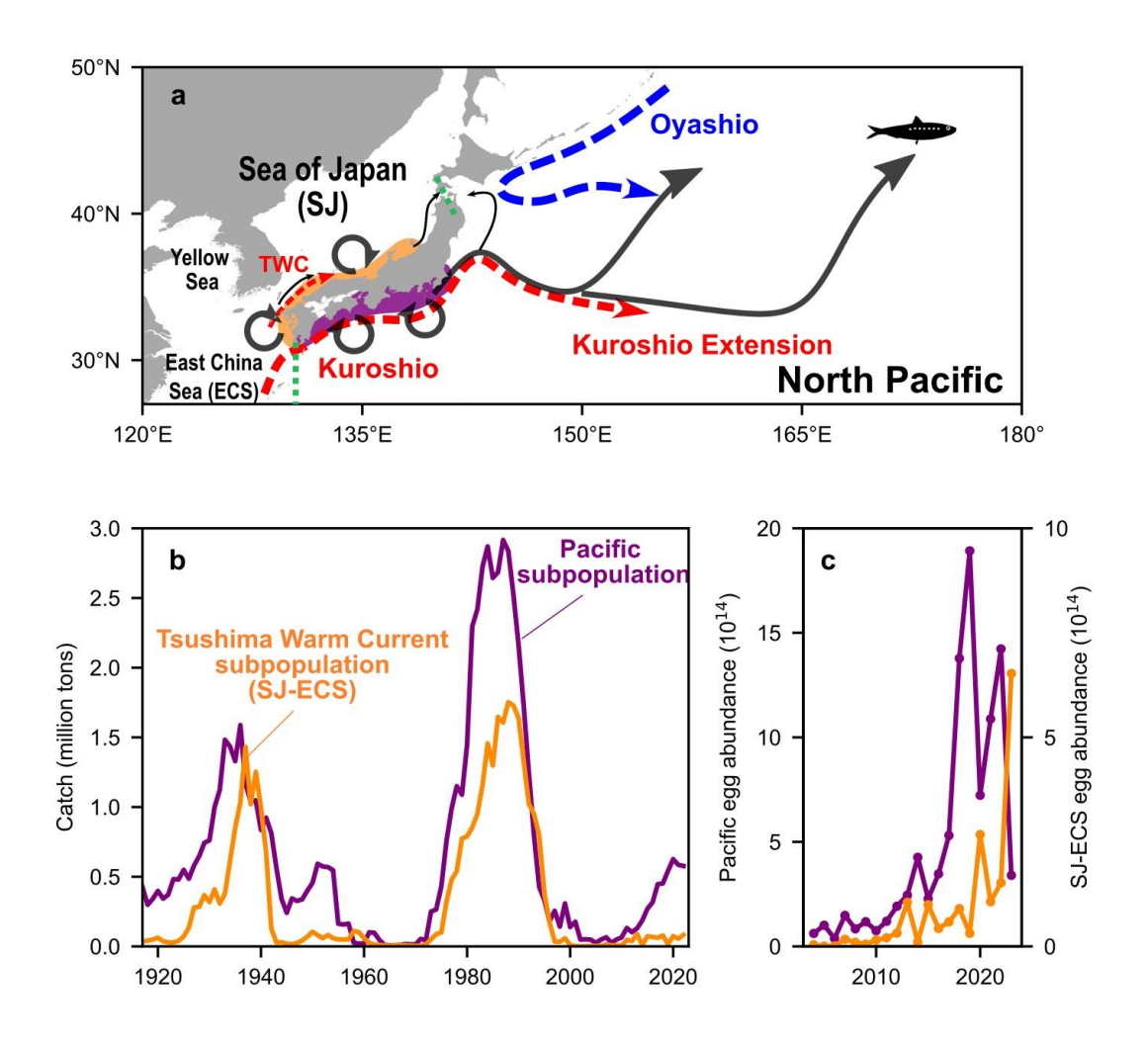


Figure 1. Hydrography and population fluctuations of Japanese sardine. Main spawning grounds in the Pacific (purple) and SJ-ECS (orange), with black arrows indicating presumed larval and juvenile movements (a). Red and blue dashed arrows represent warmer and cooler currents, respectively, and TWC denoting the Tsushima Warm Current (a). Green dotted lines mark the management boundary between the Pacific and TWC subpopulations (a). Historical Japanese sardine catch in Japan and Korea (b). Data sources are listed in Supplementary Table 1.

Results

Variations of eye lens stable isotope values in age-0 fish

The δ^{13} C and δ^{15} N values of eye lens centre for 689 age-0 sardine (< 140 mm SL in May to December) varied significantly by recruitment areas (Fig. 2a, b). Fish from the offshore Pacific (Kuroshio-Oyashio Transition Zone to the subarctic North Pacific) showed lower δ^{15} N (+1.5% to +6.5%) than those from the Sea of Japan (mostly between +8% and

+10‰) or southern coastal Pacific (+6‰ to +16‰). This pattern, lower eye lens δ^{15} N in offshore Pacific and the moderate δ^{15} N in the Sea of Japan recruits, were consistent across year-classes from 2015 to 2021 (Fig. 2c). In contrast, the δ^{15} N in the southern coastal Pacific showed apparently large inter-annual variability (Fig. 2c). Here, the spatial variation was the dominant trend, with higher δ^{15} N values in fish in or near the eutrophic inner bays with high chlorophyll concentrations, such as Osaka, Ise and Sagami Bays (Fig. 2e, f), likely reflecting the anthropogenic nutrient inputs from land and potential denitrification due to hypoxia^{23,55}. The δ^{13} C also tended to be lower in the offshore Pacific recruits and higher in the southern coastal Pacific (Fig. 2b), although the degree of geographical variation fluctuated interannually (Fig. 2d).

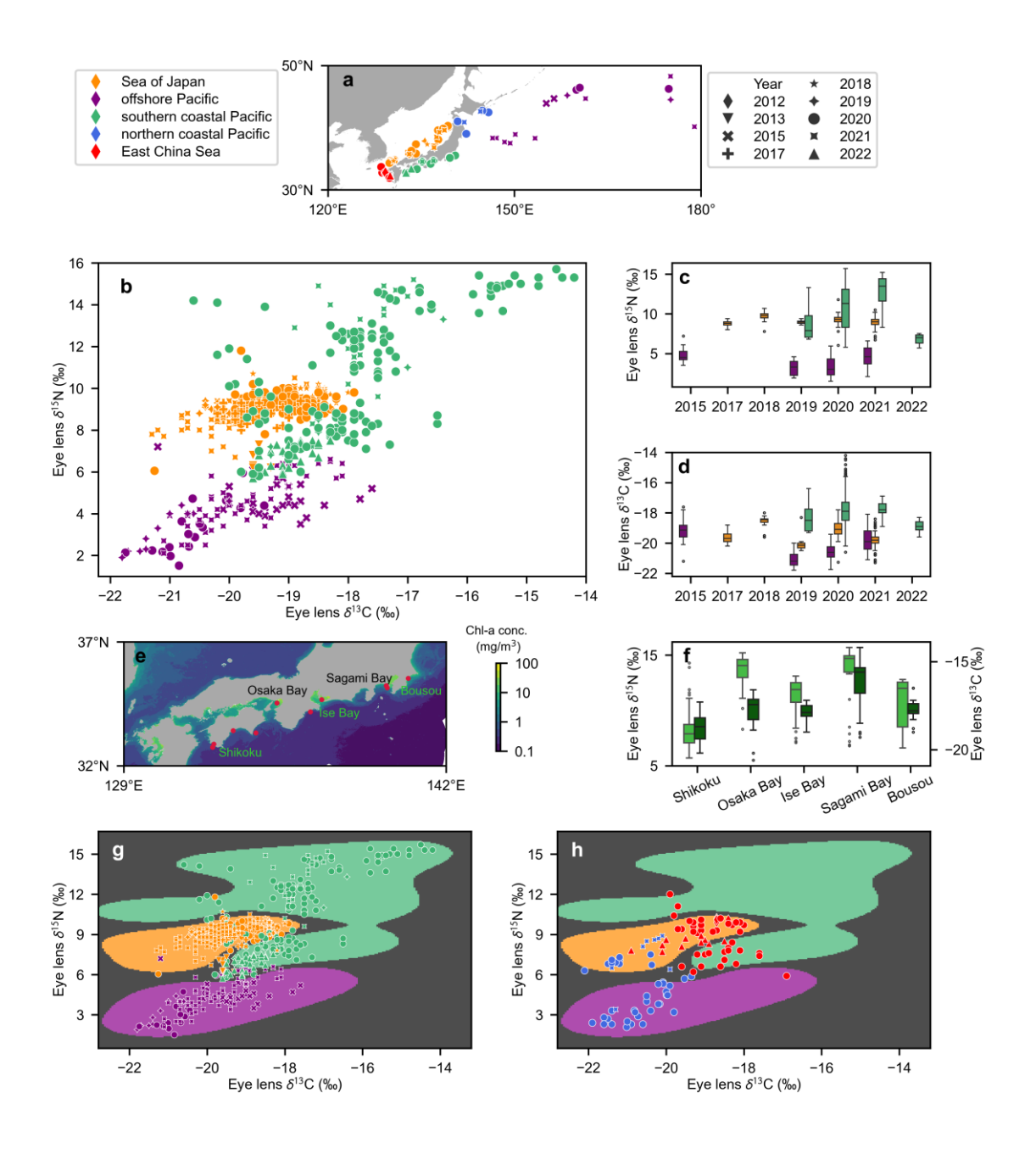


Figure 2. Isotope values of eye lens centres in sardine larvae and juveniles. Sampling locations of age-0 fish (a). The δ^{13} C and δ^{15} N of eye lens centres of age-0 fish, with colours indicating sampling areas and symbols represent years (a, b). Interannual variation of eye lens δ^{15} N (c) and δ^{13} C (d) for major recruitment areas shown as boxplots. Average satellite chlorophyll concentration during 2020 in the southern coastal Pacific, where the age-0 fish sampling points are shown as red dots (e). Spatial variation of eye lens centre δ^{15} N (left) and δ^{13} C (right) of fish from different locations in the southern coastal Pacific (f). The classification model output (background colours: purple = offshore Pacific, green = southern coastal Pacific, orange = Sea of Japan, black = prediction probability < 0.667), overlaid by the eye lens isotope values of age-0 fish from the major (g) and boundary (h) recruitment areas.

Given the significant isotope differences between recruitment areas, we developed a probabilistic classification model to predict individual nursery origins. Using 70% of the dataset from the offshore Pacific, Sea of Japan and the southern Pacific coast (584 individuals), a Gaussian Process Classifier was trained to classify fish into the three groups (background colours in Fig. 2g, h). Validation with the remaining 30% of the dataset yielded a balanced accuracy score of 0.94, indicating high classification accuracy (Table 1). The confusion matrix showed that the southern Pacific coast recruits had a 12% chance of being misclassified as Sea of Japan recruits (Table 1), reflecting marginal overlaps in isotope values (δ^{13} C: -20 to -19‰, δ^{15} N: +8 to +12‰, Fig. 2b). Age-0 fish from the northern Pacific coast and the East China Sea were generally assigned to one of the two neighbouring areas, indicative of mixing of fish or coexistence of different nursery environments, respectively (Fig. 2h). The model therefore accurately predicts nursery areas and provides a valuable tool for assessing the mixings of groups from different origin.

		Prediction	
	coastal Pacific south	Sea of Japan	offshore Pacific
coastal Pacific south	51	7	0
Sea of Japan	1	85	0
offshore Pacific	2	0	30

Observation

Table 1. Confusion matrix for the classification model tested against the validation dataset.

Mechanism driving the geographic differences in eye lens isotopes

Based on the relationship between fish size and dried whole lens diameter (Fig. 3a), eye lens centres of 0.7–1.0 mm correspond to formation from hatch to 28–42 mm SL (see Supplementary Results for details). In the larvae of this size range, muscle and eye lens isotope values were significantly correlated (δ^{15} N: Pearson's r = 0.97, p = 3.2*10⁻²⁰; δ^{13} C: Pearson's r = 0.95, p = 1.3*10⁻¹⁷), although muscle values were higher by 2.4 % in δ^{15} N and 0.1 % in δ^{13} C on average, showing a tissue-specific offset in δ^{15} N (Fig. 3b, c).

Predicted phytoplankton δ^{15} N values²⁵ during February to June, including the peak

spawning months in the SJ-ECS and Pacific^{43,44}, showed markedly low values (-1.4 to +1‰) in the Kuroshio Extension and its south. In the potential nursery areas of each recruitment group (dotted areas in Fig. 3d, e), mean values were $\pm 1.5 \pm 1.4\%$ in the offshore Pacific, $+1.8 \pm 1.0\%$ in the southern coastal Pacific and $+2.7 \pm 0.5\%$ in the Sea of Japan. Sardine larvae muscle $\delta^{15}N$ were 5–7% higher than phytoplankton across regions (Fig. 3f; south of 40°N in the offshore Pacific: $+6.8 \pm 0.7\%$, southern coastal Pacific: $+8.6 \pm 2.1\%$, Sea of Japan: $+10.3 \pm 1.6\%$), aligning with expected trophic enrichment (+3.2% per trophic interaction⁵⁶) and the trophic position of Japanese sardine (around 3)⁵⁵. Lower δ^{15} N in the offshore Pacific were more pronounced in larvae than in phytoplankton, likely because larvae isotopes reflect more localised values of the Kuroshio Extension water in which they are transported eastward 17,39. Predicted phytoplankton δ^{13} C²⁴ were relatively higher in the southern Pacific coast (-20.6 ± 0.3%), and lower in the Sea of Japan ($-21.1 \pm 0.5\%$) and offshore Pacific areas ($-21.3 \pm 0.6\%$, Fig. 3e), matching larval muscle isotope trends (Fig. 3g). Accounting for the intra-body isotope offsets (Fig. 3b, c), the eye lens centre δ^{15} N and δ^{13} C of juveniles (50 to 140 mm SL) closely matched larval muscle values (28 to 42 mm SL) across regions (Fig. 3f, g), except for δ^{15} N in the southern coastal Pacific, in the δ^{15} N varies significantly by locations (Fig. 2e, f). These findings demonstrate that the variabilities in primary producer isotopes are reflected in larval body tissues through the food chain, and preserved in the eye lens centres.

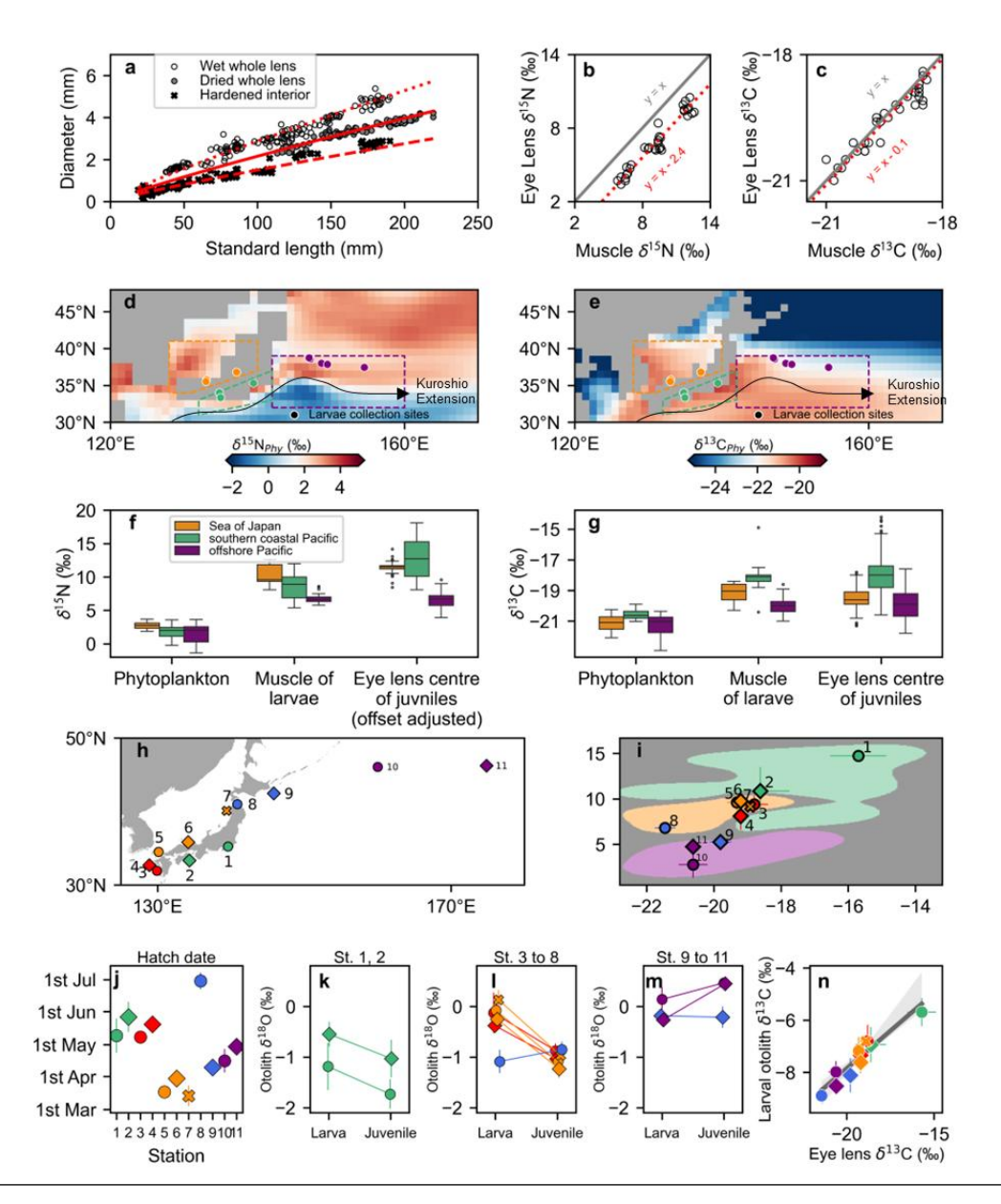


Figure 3. Mechanism of geographical variation in eye lens isotopes. Relationship between eye lens diameter and fish length, with different symbols for lens conditions, and red lines indicating the modelled allometric relationships (a). Correlations between δ^{13} C or δ^{15} N in muscle and eye lens of larvae (b, c). Modelled isoscapes of mean phytoplankton δ^{15} N (d) and δ^{13} C (e) during February to June, overlaid with sardine larvae sampling locations (circles) and potential nursery areas (dotted lines). Comparisons of δ^{15} N (f) and δ^{13} C (g) variations between phytoplankton in the potential nursery area, muscles of the larvae (28 to 42 mm SL) and eye lens centres of sardine juveniles (50 to 140 mm SL). Sampling stations of age-0 fish (2020 year-class) used for otolith and eye lens isotope comparison (h), their eye lens centre isotope values (i) and estimated hatch dates (j). The otolith δ^{18} O during larval (0 to 60 dph) and juvenile stages (106 to 120 dph) for those classified as the southern coastal Pacific (k), Sea of Japan (l) and offshore Pacific recruits (m). Relationship between eye lens centre and larval otolith δ^{13} C values (j). Points and bars indicate mean and ±1 standard deviation per station (i–n).

To further validate eye lens isotopes as a marker of geographic origin, we compared to isotopes in otoliths that were previously used as the marker³⁰, using age-0 sardine of the 2020 year-class (Fig. 3h). Their eye lens isotopes mostly covered the entire value range (Fig. 3i), and their hatch dates varied from March to July (Fig. 3j), corresponding to the spawning peak months^{43,44}. The otolith δ^{18} O at larval and juvenile stages were substantially different between recruitment groups (Fig. 3k–m). Notably, the offshore Pacific recruits, whose eye lens centre δ^{15} N were markedly low (Fig. 3i), showed significantly higher juvenile δ^{18} O than other groups (> -0.5‰, Fig. 3m), reflecting the known migration to northern cooler waters¹⁷. In addition, otolith δ^{13} C for larval stage (0 to 60 dph) varied by recruitment areas, and significantly correlated with eye lens centre δ^{13} C (Pearson's r = 0.94, n = 11, p = 1.3*10⁻⁵, Fig. 3i). As metabolised prey carbon is incorporated into otoliths⁵⁷, the correlation further supports eye lens isotopes as a proxy for prey source. This consistency demonstrates that eye lens isotope variability reflects differences in localities and migration patterns proxied by otolith isotopes, showing their comparable capability to otoliths in tracking Japanese sardine movements.

Inference of population-wide mixing

Finally, to investigated mixing patterns, we inferred the nursery origins of adult sardines (age-1 or older) using eye lens centre isotopes (Fig. 4; Supplementary Fig. 1). The 176 individuals with an assignment probability below 0.667 were excluded from the proportion estimates (Fig. 4d–f, k–m). In the western part of the southern coastal Pacific, considered as a refuge area of sardine⁵⁸, the southern coastal Pacific recruits dominated, average 75 \pm 16% (1SD) (Fig. 4k). In contrast, in the eastern part, where over 95% of recent Pacific-side spawning occurs⁴⁶, was dominated by offshore Pacific recruits (83 \pm 14%) during the January to June spawning seasons, with minor contributions (10 \pm 9%) from the southern coastal Pacific recruits (Fig. 4l). Offshore Pacific recruits also made up $80 \pm 11\%$ of the northern Pacific fishing ground (Fig. 4m). The proportions on the Pacific side showed limited interannual variations during 2019 to 2023, supporting the hypothesis that offshore Pacific recruits originating from the eastern spawning ground primarily drove the recent population increase in the Pacific⁴⁴.

Surprisingly, many adults caught in the SJ-ECS were classified as offshore Pacific recruits, challenging the conventional view of two semi-discrete subpopulations (Fig. 4a-c). Most

adults collected in the eastern Sea of Japan from January to June during 2019 to 2023 were classified as offshore Pacific recruits ($85 \pm 10\%$ on average) due to lower eye lens δ^{13} C and δ^{15} N (Fig. 4f). In the western Sea of Japan during 2020 to 2023, the offshore Pacific recruits dominated except for 2021 ($91 \pm 7\%$), when Sea of Japan recruits accounted for $95 \pm 9\%$ (Fig. 4e). The East China Sea contained both individuals classified as Sea of Japan or southern coastal Pacific recruits before 2022 (Fig. 4d). As this is similar pattern with the age-0 in the East China Sea (Fig. 2h), it is not necessarily indicative of fish migrations from the two areas. However, in 2023, when the egg abundance in the SJ-ECS sharply increased (Fig. 1c), offshore Pacific recruits become predominant ($93 \pm 5\%$) (Fig. 4d).

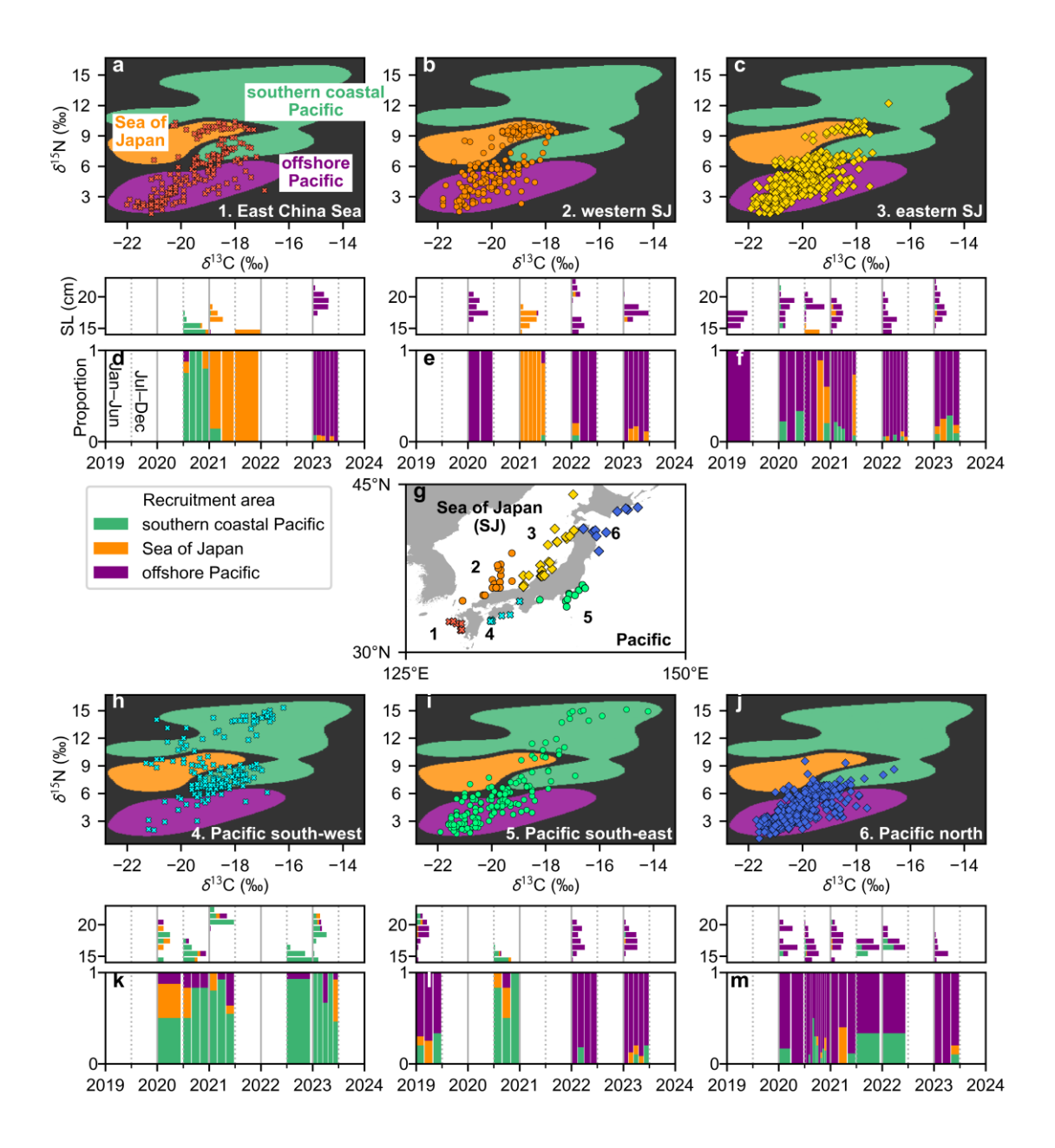


Figure 4. Population-wide mixing from different recruitment sources. The δ^{13} C and δ^{15} N values of eye lens centres of adults from the East China Sea (a), western Sea of Japan (b) and eastern Sea of Japan (c), overlaid on classification model background colours (Figure 2g, h). Proportion of fish from three nursery areas in each region (d–f), with each bar representing a sampling batch (6–20 individuals), sorted by date and grouped into half-year blocks (d–f). Length frequency for each block is shown above (d–f). Sampling locations of adults (g). Isotope values of fish from the western (h) and eastern (i) part of the southern coastal Pacific, and the northern coastal Pacific (j), and the temporal variation of the proportion (k–m). The counts of each recruitment group are shown in Supplementary Fig. 1.

Discussion

This study demonstrates that δ^{13} C and δ^{15} N values in the eye lens centre are effective markers of nursery origin in marine fish. A potential limitation is the possible similarity of isotope values between fish from different nursery areas. In Japanese sardine, mixing inferences could be affected if unsampled areas, such as the northern Sea of Japan or the Yellow Sea where eggs may be present in low abundances^{53,59}, show isotope values similar to the offshore Pacific recruits. However, modelled phytoplankton $\delta^{15}N$ in the Kuroshio and the Kuroshio Extension are exceptionally low (-1.4% to +1%) due to active nitrogen fixation, distinguishing it from the potential nursery areas (Fig. 3d; Yoshikawa et al., 2024). While the northern Sea of Japan can show moderately low phytoplankton δ^{15} N values (+1 to +2%) that can partially overlap with values around the Kuroshio (Fig. 3d), phytoplankton δ^{13} C is several permill lower there due to lower temperature (Fig. 3e), which should enable discrimination in δ^{13} C- δ^{15} N biplot. Coastal estuaries, which are harder to model, generally have higher $\delta^{15}N$ than offshore waters⁵⁵ (Fig. 2f). Since baseline isotope variation is transferred through the food chain and recorded in eye lenses (Fig. 3f, g), overlaps with the low δ^{15} N in the Pacific offshore are not very likely. Consistency with the otolith isotopes³⁰ also reduces the chance of systematic confusion (Fig. 3k-m). Combined with a mechanistic understanding of isotope variability, simple chemical analysis of the eye lens centre enables robust inference of nursery origin, and assessments of complex mixing processes.

Despite Nakai's⁵² early suggestion of connectivity, research and stock assessments have long assumed limited sardine migration from the Pacific to the SJ-ECS^{45-48,53}. However, our eye lens isotope analysis, consistent with mitochondrial DNA⁵⁴ and otolith isotope³⁰ studies, support significant migration of Pacific recruit to the SJ-ECS, thereby reinforcing Nakai's hypothesis⁵². Long-distance migrations from the original nursery to foreign areas, with potential reproduction at the destination, have been suggested for sardine populations in the northeast Pacific and southeast and northeast Atlantic^{15,60,61}. Japanese sardine was even reported off California coast in 2022, likely crossing the entire North Pacific¹⁶, highlighting the exceptional migratory capacity for a small pelagic fish. Due to their highly-efficient filter-feeding apparatus⁶², surrounding prey zooplankton density and growth rates decrease as population increases^{33,49}. Such density-dependent effects may drive migration to alternative foraging areas to maintain fitness^{61,63}. Importantly, the decrease in sardine growth in the SJ-ECS during 2010s had been less severe than in the Pacific⁵⁰, which has been pointed as evidence against the mixing (Fisheries Research and

Education Agency, personal communication). However, this can be explained by compensatory growth i.e., accelerated growth when favourable conditions are restored after a period of growth depression, a well-documented phenomenon in fishes⁶⁴. The mesozooplankton biomass in the SJ-ECS decreased but remained in moderate level in 2010s³³, which may had released the growth-depressed Pacific migrants from competition and allowed them to catch up in size, resulting in the recovery of size-at-age in the SJ-ECS.

Our large sample size enabled us to track the interannual variation in migration behaviour, which likely plays a key role in sardine population dynamics. The shifts in dominant groups in the western Sea of Japan from 2020 to 2021 and 2021 to 2022 suggest that offshore Pacific recruits migrating to the SJ-ECS is generally consistent but can occasionally pause or even reverse. The fluctuations in egg abundances on both sides support this view (Fig. 1c). While both had increased since the 2000s, their detrended values by differencing show a significant negative correlation (Pearson's r = -0.78, p = $7.5*10^{-5}$, n = 19), indicating a shared pool of spawners with interannual variation in regional contribution. Abrupt declines of fishery catch and egg abundance in the SJ-ECS were observed in 2014 and 2019³⁰, when the egg abundance showed spiky increases in the Pacific (Fig. 1c). This suggests that most adults that were in the SJ-ECS in the previous year had moved back to the Pacific, and, migrations otherwise were limited. Furthermore, in 2023 Pacific egg abundance sharply decreased and was surpassed by SJ-ECS level. This coincided with offshore Pacific recruits expanding to the East China Sea (Fig. 4d-f), reflecting a massive migration to the SJ-ECS. The population synchroneity in the western North Pacific and the SJ-ECS observed for a century (Fig. 1b) is therefore likely a result of such migration behaviour: the offshore Pacific recruits moving among the region and reproducing, thereby actively linking the two systems.

Our findings have important implications for fisheries managements. Current stock assessments for the Pacific and the SJ-ECS sardine subpopulations carry significant uncertainties, as migrations between them is not accounted for. More accurate assessments may require models explicitly considering the mixing or assume a single, inter-connected population. However, if egg abundance in the SJ-ECS continues to rise (Fig. 1c), the contribution of Sea of Japan recruits may increase. This could lead to the emergence of an apparently self-recruiting population, despite its initial support from

Pacific migrants. Therefore, continuous monitoring of fish nursery origins and the analysis of archived samples in the previous high-biomass periods are essential. For future predictions, offshore Pacific recruitment likely plays the most critical role in overall population fluctuations. Larval survival in this region had been linked to the intensity of winter mixing near the Kuroshio axis, which influences food availability in spring³⁹. While empirical confirmation remains limited, the low δ^{15} N in eye lenses of offshore Pacific recruits indicate their larval growths depends on primary production using Kuroshio-derived light nitrogen²⁵, partially supporting the hypothesis. Further investigation into interannual variations in food chain length and energy transfer efficiency, using the compound specific isotopic analysis of amino acids, could deepen the understanding of the bottom-up processes⁶⁵.

Intense sardine migration can have significant ecological and biogeochemical consequences at the destination. In the Sea of Japan, mesozooplankton biomass severely decreased during sardine booms in the 1970-80s and late 2010s due to increased predation pressure³³. This had likely supressed other major zooplankton feeders in SJ-ECS, such as anchovy Engraulis japonicus and Japanese common squid Todarodes pacificus, whose abundance also decreased during these periods (Supplementary Fig. 2). Sardines have likely sustained their abundance by recruiting from the offshore Pacific rather than relying solely on local reproduction, allowing them to avoid the effect of prey depletion in the Sea of Japan during early life stages. This makes the marginal sea a rare case where a trophic cascade is governed by the migration of small pelagic fish from external systems. As a result, a larger biomass of zooplankton feeders, beyond what regional primary production alone could sustain, may be present in the Sea of Japan, which can enhance productions of pelagic fish predators and benthic detritus feeders. In South Africa, massive sardine migrations from productive to oligotrophic areas serve as a major nutrient source, potentially exceeding inputs from local upwelling and freshwater inputs⁶⁶. Similarly, just as Salmonidae transport marine-derived nutrients to freshwater systems⁶⁷, the migration of abundant mid-trophic fish like sardine may play an overlooked role in redistributing nutrients across marine ecosystems, warranting further studies.

Overall, this study demonstrated that eye lens isotopes can provide unique insights into marine fish population dynamics. Compared to natural tags such as otolith chemistry and genomics, eye lens isotope analysis can be more accessible and cost-effective, making the resource- and time-intensive task of mixing assessments more feasible. The analysis can also resolve year-by-year changes in population structure that may occur under rapid climate change, in contrast to genetic methods. It is widely applicable beyond bony fishes, extending to cephalopods²⁹, sharks and rays⁶⁸, and even birds⁶⁹. This scalability and utility may commoditise studies of marine organism movements and enhance intra- and international discussions towards biologically sound management strategies. The effectiveness of eye lens isotopes as a geographical marker should vary by region and fish life-cycles, which should be tested in future. However, strong spatial gradients in phytoplankton δ^{13} C and δ^{15} N exists across diverse environments, particularly near river inputs, estuaries, coastal upwelling areas, nitrogen fixation and subarctic fronts^{22-25,55} where various marine organisms often aggregate, which highlights the potential of the method's broad applicability. Despite the potential to link biogeochemical cycles, marine behavioural ecology and ecosystem-based managements, eye lenses have not been routinely collected and archived like hard tissues. We strongly encourage research institutes to begin collecting and storing animal eye lenses frozen to support future studies.

Materials and methods

Sample collection and eye lens processing

Sardine samples were collected by commercial perse-seiner and coastal set-net fisheries or scientific cruise surveys using mid-water trawls during 2012 to 2023. Based on the typical growth rate of the species^{46,47}, fish smaller than 140 mm Standard Length (SL) caught during late-spring to autumn (May to December) were considered as age-0. Age-0 fish, 689 in total, were mainly collected in cruise surveys in the offshore Pacific and Sea of Japan and fisheries in other areas during summer and autumn, when juveniles have broadest distribution extending from the Japanese coast to the offshore subarctic Pacific¹⁷. The adults (≥ 140 mm SL), 1432 in total, were mainly collected from fisheries during winter to spring when they approach the coast for spawning, and also from the northern Pacific coastal areas which is the main fishing ground for the species⁴⁶. Sampling aimed to cover key recruitment and spawning areas, although access to samples from the northern SJ and the Sea of Okhotsk, known as part of feeding grounds for adults during summer⁵³, was limited. Fish were frozen on land or on board at −20°C for preservation until being thawed for dissection. In the laboratory, length and weight of fish were measured to the nearest 1 mm and 0.1 g, respectively, and the sex was recorded when

possible. From up to 20 individuals each sampling batch, eye lenses were extracted using forceps and were frozen in plastic 96-well plates.

Eye lenses were placed on a slide glass under a stereo microscope with a micrometre scale for delamination. Using forceps, gelatinous cortex and outer laminae were removed until the diameter of the remaining lens became smaller than 1 mm, typically 0.7 to 0.9 mm, under 10-20X magnification. The remaining centre part was rinsed with milli-Q water to remove the potentially tangled fibres from outer laminae, then placed in the bottom of tin capsules (Shoko Science Co., Ltd.). The capsules were air-dried for more than a week, then folded and inserted to DELTA plus Advantage coupled with FLASH2000 system in Geo Science Laboratory, Nagoya, Japan for δ^{13} C and δ^{15} N analysis. The analytical precisions were \pm 0.1‰ for δ^{13} C and \pm 0.2‰ for δ^{15} N.

Data analysis of eye lens isotopes

We developed a classification model based on the eye lens isotope data of age-0 recruits from different recruitment areas, and inferred the nursery origins of the adults using it. Recruitment areas were divided into three primary regions where juveniles are commonly found in summer and autumn—the offshore Pacific (Kuroshio-Oyashio Transition Zone to the subarctic North Pacific), the Sea of Japan, and southern coastal Pacific—along with two marginal areas between them: the northern coastal Pacific and the East China Sea (Fig. 2). In the northern coastal Pacific, fish from the Pacific and Sea of Japan can be mixed⁵³. In the East China Sea, the narrow zone influenced by both the Kuroshio and Tsushima Warm Current allows prey and fish isotopes similar to those in the Sea of Japan or southern coastal Pacific to coexist. Data from these marginal areas were therefore excluded from classifier development, allowing data from the primary regions to better represent the species' nursery environments. The remaining age-0 dataset (n = 584) was randomly divided into a training dataset (70%) and a validation set (30%). To account for the complex data distribution, the Gaussian Process Classifier was fit to the training dataset by using the Radial Basis Function kernel with default parameters in the scikitlearn library 1.2.2 based on Python 3.9.18. Model accuracy was assessed using a confusion matrix and total accuracy on the validation set. Finally, the recruitment areas of adults were inferred from the eye lens δ^{13} C and δ^{15} N values to assess the populationwide mixing.

Relationship between sardine size and eye lens diameter

The relationship between eye lens diameter and fish length was established to reconstruct fish size at the formation of a delaminated eye lens. Fish eye lenses consist of outer gelatinous cortex and inner hardened regions, with the cortex gradually dehydrating to form the outer hardened interior as the fish grows⁷⁰. The relationship between fish length and the diameter of dried whole eye lens is likely most suitable for reconstructing fish size, although drying eye lenses without considerable deformation are only possible for those from fresh fish, which are of limited availability. To address this, we extracted eye lenses from 137 fresh and 156 frozen sardines and measured diameters in three conditions: wet whole lens, dried whole lens, and hardened interior. Assuming allometric relationships between fish length and lens diameters, and a consistent ratio of these diameters throughout growth⁷⁰, we modeled their relationship using a linear random-effects model (see Supplementary Methods for details).

Isotopic offset between eye lenses and muscles

We assessed isotopic offsets between eye lenses and muscle during the larval stage to improve comparisons across tissues. While muscle isotope values reflect recent prey before turnover, whole eye lenses integrate isotopic signals over a lifetime. However, during the larval stage, this difference in timescales is minimized, allowing direct comparison of isotope values. We collected 33 frozen larvae (28–42 mm SL) from cruise surveys and fisheries, extracting dorsal muscles and whole eye lenses. Lipids were removed from muscle samples using a 2:1 chloroform-methanol solution before isotope analysis. Isotope values were measured using a DELTA plus Advantage coupled with a FLASH2000 system at Geo Science Laboratory, Nagoya, Japan.

Validations as a geographical marker

To investigate the drivers of geographical variation in eye lens isotopes, we compared trends in eye lens isotope values with the 2020 satellite-derived chlorophyll-a distribution and model-predicted annual-mean phytoplankton $\delta^{15}N^{25}$ and $\delta^{13}C^{24}$. The isoscape models couple ocean circulation models with biogeochemical processes relevant to isotopic variability, and are calibrated against available observations. In addition, the $\delta^{13}C$ and $\delta^{15}N$ values of muscles of 71 larvae between 28 to 42 mm SL, corresponding to the size range at eye lens centre (0.7 to 1.0 mm) formation, collected in the offshore Pacific, Sea

of Japan and southern coastal Pacifics between 2001 and 2023 were extracted from the archived dataset used in Sakamoto et al⁵⁵. Comparing larval muscle isotope values with eye lens centre isotopes in juveniles allowed us to test whether larval prey isotopes are retained and preserved in the eye lens centre as the fish grow.

We also tested the consistency of eye lens isotopes with otolith isotopes. Otolith carbon originates from both metabolised prey and dissolved inorganic carbon in seawater⁵⁷. If eye lens isotopes primarily reflect prey sources, a positive correlation is expected between δ^{13} C in the eye lens centre and the otolith portion formed during larval stage. In addition, otolith δ^{18} O during juvenile stage has been used to identify Japanese sardine recruitment areas, as it reflects temperature differences between regions³⁰. If geographic variations in eye lens isotopes align with juvenile otolith δ^{18} O trends, they can serve as a robust and efficient marker of nursery origins. For comparison, we analysed the 2020 year-class, selecting up to six individuals from 11 stations across recruitment areas (52 total) from age-0 fish captured between August and November 2020. Otolith δ^{13} C (0–60 days post-hatch (dph)) and δ^{18} O (106–120 dph) were analysed following Sakamoto et al.³⁰ and compared to δ^{13} C and δ^{15} N of eye lens centre, respectively. See Supplementary Information for detailed protocols.

Conflict of interest statement

The authors have no conflicts of interest to declare.

Acknowledgement

This study is supported by the Research and assessment program for fisheries resources, the Fisheries Agency of Japan, and MEXT/JSPS KAKENHI (Japan) Grant numbers 22H05028, 22H05029, 23H02288, and 19J00793. We are grateful to Miyu Yukiyama (Ezh Inc.) for contributions to sample collections. We appreciate Chisato Yoshikawa (JAMSTEC) for providing phytoplankton isotope data. This paper is also a contribution to the international ICES-PICES Working Group on Sustainable Pelagic Forage Communities (ICES WGSPF, PICES WG53).

Author contributions

Conceptualization: TS, MT Methodology: TS, KS, SK, TI

Investigation: TS Visualization: TS

Funding acquisition: TS, MT, TI, KS

Project administration: MT

Supervision: MT, KS

Writing – original draft: TS

Writing – review & editing: TS, MT, KS, SK, TI

References

- 1. Boyd, C. E., McNevin, A. A. & Davis, R. P. The contribution of fisheries and aquaculture to the global protein supply. Food Security 14, 805–827 (2022).
- 2. Majluf, M., Matthews, M., Pauly, P., Skerritt, S. & Palomares, P. A review of the global use of fishmeal and fish oil and the Fish In:Fish Out metric. Sci. Adv. 10, eadn5650 (2024).
- 3. Chavez, F. P., Ryan, J., Lluch-Cota, S. E. & Niquen, C. M. From anchovies to sardines and back: multidecadal change in the Pacific Ocean. Science 299, 217–221 (2003).
- 4. Rykaczewski, R. R. & Checkley, D. M., Jr. Influence of ocean winds on the pelagic ecosystem in upwelling regions. Proc. Natl. Acad. Sci. USA. 105, 1965–1970 (2008).
- 5. Essington, T. E. *et al.* Fishing amplifies forage fish population collapses. Proc. Natl. Acad. Sci. USA 112, 6648–6652 (2015).
- 6. Campana, C. et al. Mortality drives production dynamics of Atlantic cod through 1100 years of commercial fishing. Sci. Adv. 11, eadt4782 (2025).
- 7. Sugihara, G. et al. Detecting causality in complex ecosystems. Science 338, 496-500 (2012).
- 8. Ma, S. et al. Non-stationary effects of multiple drivers on the dynamics of Japanese sardine (*Sardinops melanostictus*, Clupeidae). Fish Fish. 24, 40-55 (2023).
- 9. Rooker, J. R. et al. Natal homing and connectivity in Atlantic bluefin tuna populations. Science 322, 742-744 (2008).
- 10. Sakamoto, T. et al. Contrasting life-history responses to climate variability in eastern and western North Pacific sardine populations. Nat. Commun. 13, 5298 (2022).
- 11. Trueman, C. N. et al. Thermal sensitivity of field metabolic rate predicts differential futures for bluefin tuna juveniles across the Atlantic Ocean. Nat. Commun. 14, 7379 (2023).

- 12. Cadrin, S. X. Defining spatial structure for fishery stock assessment. Fish. Res. 221, 105397 (2020).
- 13. Hilborn, R. et al. Effective fisheries management instrumental in improving fish stock status. Proc. Natl. Acad. Sci. USA 117, 2218-2224 (2020).
- 14. Block, B. A. et al. Tracking apex marine predator movements in a dynamic ocean. Nature 475, 86-90 (2011).
- 15. Teske, P. R. et al. The sardine run in southeastern Africa is a mass migration into an ecological trap. Sci. Adv. 7, eabf4514 (2021).
- 16. Longo, G. C. et al. Crossing the Pacific: Genomics Reveals the Presence of Japanese Sardine (*Sardinops melanosticta*) in the California Current Large Marine Ecosystem. Mol. Ecol. 33, e17561 (2024).
- 17. Sakamoto, T. et al. Combining microvolume isotope analysis and numerical simulation to reproduce fish migration history. Methods Ecol Evol 10, 59–69 (2019).
- 18. Campana, S. E., Chouinard, G. A., Hanson, J. M., Fréchet, A. & Brattey, J. Otolith elemental fingerprints as biological tracers of fish stocks. Fish. Res. 46, 343–357 (2000).
- 19. Balbar, A. C. & Metaxas, A. The current application of ecological connectivity in the design of marine protected areas. Glob. Ecol. Conserv. 17, e00569 (2019).
- 20. Wallace, A. A., Hollander, D. J. & Peebles, E. B. Stable isotopes in fish eye lenses as potential recorders of trophic and geographic history. PLoS One 9, e108935 (2014).
- 21. Yoshikawa, C. *et al.* Nitrogen and carbon isotopic relationships in the diet and eye lenses of chub mackerel revealed in a laboratory rearing experiment. Prog. Earth Planet. Sci. 12, 57 (2025).
- 22. Goericke, R. & Fry, B. Variations of marine plankton δ13C with latitude, temperature, and dissolved CO2 in the world ocean. Glob. Biogeochem. Cycles 8, 85-90 (1994).
- 23. Voss, M., Dippner, J. W. & Montoya, J. P. Nitrogen isotope patterns in the oxygen-deficient waters of the Eastern Tropical North Pacific Ocean. Deep Sea Res. Part I Oceanogr. Res. Pap. 48, 1905–1921 (2001).
- 24. Magozzi, S., Yool, A., Vander Zanden, H. B., Wunder, M. B. & Trueman, C. N. Using ocean models to predict spatial and temporal variation in marine carbon isotopes. Ecosphere 8, e01763 (2017).
- 25. Yoshikawa, C., Shigemitsu, M., Yamamoto, A., Oka, A. & Ohkouchi, N. A nitrogen isoscape of phytoplankton in the western North Pacific created with a marine nitrogen isotope model. Front. Mar. Sci. 11, 1294608 (2024).
- 26. Vecchio, J. L. & Peebles, E. B. Spawning origins and ontogenetic movements for demersal fishes: An approach using eye-lens stable isotopes. Estuar. Coast. Shelf Sci.

- 246, 107047 (2020).
- 27. Harada, Y. et al. Compound-Specific Nitrogen Isotope Analysis of Amino Acids in Eye Lenses as a New Tool to Reconstruct the Geographic and Trophic Histories of Fish. Front. Mar. Sci. 8, 2146 (2022).
- 28. Wallace, A. A., Ellis, G. S. & Peebles, E. B. Reconstructions of individual fish trophic geographies using isotopic analysis of eye-lens amino acids. PLoS One 18, e0282669 (2023).
- 29. Sakamoto, T. et al. Stable isotopes in eye lenses reveal migration and mixing patterns of diamond squid in the western North Pacific and its marginal seas. ICES J. Mar. Sci. 80, 2313-2328 (2023).
- 30. Sakamoto, T., Takahashi, M., Shirai, K., Aono, T. & Ishimura, T. Fisheries shocks provide an opportunity to reveal multiple recruitment sources of sardine in the Sea of Japan. Sci. Rep. 14, 21722 (2024).
- 31. Checkley Jr, D. M., Asch, R. G. & Rykaczewski, R. R. Climate, anchovy, and sardine. Annu. Rev. Mar. Sci. 9, 469-493 (2017).
- 32. Cury, P. M. et al. Global seabird response to forage fish depletion--one-third for the birds. Science 334, 1703-1706 (2011).
- 33. Kodama, T., Igeta, Y. & Iguchi, N. Long-Term Variation in Mesozooplankton Biomass Caused by Top-Down Effects: A Case Study in the Coastal Sea of Japan. Geophys. Res. Lett. 49, e2022GL099037 (2022).
- 34. Fuji, T. et al. Biological interactions potentially alter the large-scale distribution pattern of the small pelagic fish, Pacific saury *Cololabis saira*. Mar. Ecol. Prog. Ser. 704, 99–117 (2023).
- 35. Walker, W. A. Summer feeding habits of Dall's porpoise, *Phocoenoides dalli*, in the southern Sea of Okhotsk. Mar. Mamm. Sci. 12, 167–181 (1996).
- 36. Senzaki, M. et al. Long-term declines in common breeding seabirds in Japan. Bird Conserv. Int. 30, 434–446 (2020).
- 37. Schwartzlose, R. A. et al. Worldwide large-scale fluctuations of sardine and anchovy populations. S. Afr. J. Mar. Sci. 21, 289–347 (1999).
- 38. Takahashi, M., Watanabe, Y., Yatsu, A. & Nishida, H. Contrasting responses in larval and juvenile growth to a climate–ocean regime shift between anchovy and sardine. Can. J. Fish. Aquat. Sci. 66, 972–982 (2009).
- 39. Nishikawa, H. et al. Winter mixed layer depth and spring bloom along the Kuroshio front: implications for the Japanese sardine stock. Mar. Ecol. Prog. Ser. 487, 217–229 (2013).
- 40. Takasuka, A., Oozeki, Y. & Aoki, I. Optimal growth temperature hypothesis: Why do

- anchovy flourish and sardine collapse or vice versa under the same ocean regime? Can. J. Fish. Aquat. Sci. 64, 768–776 (2007).
- 41. Kuroda, H. et al. Unconventional Sea Surface Temperature Regime Around Japan in the 2000s–2010s: Potential Influences on Major Fisheries Resources. Front. Mar. Sci. 7 (2020).
- 42. Oozeki, Y., Takasuka, A., Kubota, H. & Barange, M. Characterizing Spawning Habitats of Japanese Sardine, *Sardinops melanostictus*, Japanese Anchovy, *Engraulis japonicus*, and Pacific Round Herring, *Etrumeus teres*, in the Northwestern Pacific. CalCOFI Rep. 48, 191 (2007).
- 43. Furuichi, S. et al. Disentangling the effects of climate and density-dependent factors on spatiotemporal dynamics of Japanese sardine spawning. Mar. Ecol. Prog. Ser. 633, 157–168 (2020).
- 44. Niino, Y., Furuichi, S., Kamimura, Y. & Yukami, R. Spatiotemporal spawning patterns and early growth of Japanese sardine in the western North Pacific during the recent stock increase. Fish. Oceanogr. 30, 643-652 (2021).
- 45. Wada, T. & Jacobson, L. D. Regimes and stock-recruitment relationships in Japanese sardine (*Sardinops melanostictus*), 1951-1995. Can. J. Fish. Aquat. Sci. 55, 2455-2463 (1998).
- 46. Furuichi, S. et al. Stock assessment and evaluation for the Pacific stock of Japanese sardine (fiscal year 2023). In Marine fisheries subpopulation assessment and evaluation for Japanese waters. Japan Fisheries Agency and Japan Fisheries Research and Education Agency, Tokyo, 52pp (2024). https://abchan.fra.go.jp/wpt/wpcontent/uploads/2024/03/details_2023_01.pdf
- 47. Muko, S. et al. Stock assessment and evaluation for the Tsushima Warm Current stock of Japanese sardine (fiscal year 2023). In Marine fisheries subpopulation assessment and evaluation for Japanese waters. Japan Fisheries Agency and Japan Fisheries Research and Education Agency, Tokyo, 61pp (2024). https://abchan.fra.go.jp/wpt/wp-content/uploads/2024/03/details_2023_02.pdf
- 48. Kodama, T. et al. Improvement in recruitment of Japanese sardine with delays of the spring phytoplankton bloom in the Sea of Japan. Fish. Oceanogr. 27, 289–301 (2018).
- 49. Kamimura, Y., Tadokoro, K., Furuichi, S. & Yukami, R. Stronger density-dependent growth of Japanese sardine with lower food availability: Comparison of growth and zooplankton biomass between a historical and current stock-increase period in the western North Pacific. Fish. Res. 255, 106461 (2022).
- 50. Fujinami, Y., Takahashi, M. & Kurota, H. Evaluation of the Precision of Age Determination and Variability in Growth for Japanese Sardine (Sardinops

- melanostictus), Tsushima Warm Current Subpopulation. JARQ 58, 65–74 (2024).
- 51. Inoue, M. et al. Kuroshio fractions in the southwestern sea of Japan; implications from radium isotopes. Cont. Shelf Res. 214, 104328 (2021).
- 52. Nakai, Z. Studies relevant to mechanisms underlying the fluctuation in the catch of the Japanese sardine, *Sardinops melanostictus*. Jap. J. Ichthyol. 9, 1-115 (1962).
- 53. Kuroda, K. Studies on the recruitment process focusing on the early life history of the Japanese sardine, *Sardinops melanostictus* (Schlegel). Bull. Natl. Res. Inst. Fish. Sci. 3, 25–278 (1991).
- 54. Okazaki, T., Kobayashi, T. & Uozumi, Y. Genetic relationships of pilchards (genus: *Sardinops*) with anti-tropical distributions. Mar. Biol. 126, 585-590 (1996).
- 55. Sakamoto, T. et al. Geographic, seasonal and ontogenetic variations of δ^{15} N and δ^{13} C of Japanese sardine explained by baseline variations and diverse fish movements. Prog. Oceanogr. 219, 103163 (2023).
- 56. Sweeting, C. J., Barry, J., Barnes, C., Polunin, N. & Jennings, S. Effects of body size and environment on diet-tissue $\delta^{15}N$ fractionation in fishes. J. Exp. Mar. Biol. Ecol. 340, 1–10 (2007).
- 57. Solomon, C. T. et al. Experimental determination of the sources of otolith carbon and associated isotopic fractionation. Can. J. Fish. Aquat. Sci. 63, 79–89 (2006).
- 58. Ishida, M. Rapid decrease of egg production of Pacific stock of Japanese sardine, *Sardinops melanostictus*, and characteristics of persistent spawning ground in Tosa Bay, southwestern Japan. Bull. Jpn. Soc. Fish. Oceanogr. (2006).
- 59. Sokolovskaya, T. G., Sokolovsky, A. S. & Epur, I. V. Species composition and seasonal variations of ichthyoplankton of the coastal zone of Vostok Bay (Peter the Great Bay, Sea of Japan) collected at light stations. Russ. J. Mar. Biol. 36, 125-132 (2010).
- 60. Lo, N. C., Macewicz, B. J. & Griffith, D. A. Migration of Pacific sardine (*Sardinops sagax*) off the west coast of United States in 2003–2005. Bull. Mar. Sci. 87, 395-412 (2011).
- 61. Silva, A. et al. Adult-mediated connectivity and spatial population structure of sardine in the Bay of Biscay and Iberian coast. Deep Sea Res. Part II Top. Stud. Oceanogr. 159, 62-74 (2019).
- 62. Van der Lingen, C. D., Hutchings, L. & Field, J. G. Comparative trophodynamics of anchovy *Engraulis encrasicolus* and sardine *Sardinops sagax* in the southern Benguela: are species alternations between small pelagic fish trophodynamically mediated? Afr. J. Mar. Sci. 28, 465–477 (2006).
- 63. Shepherd, T. D. & Litvak, M. K. Density-dependent habitat selection and the ideal

- free distribution in marine fish spatial dynamics: considerations and cautions. Fish Fish. 5, 141–152 (2004).
- 64. Ali, M., Nicieza, A. & Wootton, R. J. Compensatory growth in fishes: a response to growth depression. Fish Fish. **4**, 147–190 (2003).
- 65. Swalethorp, R. et al. Anchovy boom and bust linked to trophic shifts in larval diet. Nat. Commun. 14, 7412 (2023).
- 66. Hutchings, L. et al. Ecosystem considerations of the KwaZulu-Natal sardine run. Afr. J. Mar. Sci. 32, 413-421 (2010).
- 67. Naiman, R. J., Bilby, R. E., Schindler, D. E. & Helfield, J. M. Pacific Salmon, Nutrients, and the Dynamics of Freshwater and Riparian Ecosystems. Ecosystems 5, 399–417 (2002).
- 68. Kuntz, J. P. *et al.* Investigating eye lens composition for stable isotope analysis in fishes: a comparison between Chondrichthyes and Actinopterygii. Environ. Biol. Fishes 108, 515–532 (2025).
- 69. Hasegawa, E. A. *et al.* Isotope analysis of birds' eye lens provides early-life information. Prog. Earth Planet. Sci. 12, 9 (2025).
- 70. Leifsdóttir, R. R. & Campana, S. E. Species independence of eye lens dimensions in teleosts and elasmobranchs. PLoS One 18, e0286388 (2023).

Supplementary Information for: Eye lens isotope tag reveal migration as a driver of Japanese sardine synchrony

Authors

Tatsuya Sakamoto^{1,2*}, Motomitsu Takahashi¹, Kotaro Shirai³, Satoshi Kitajima¹, Toyoho Ishimura⁴

- 1. Fisheries Resources Institute, Japan Fisheries Research and Education Agency, Nagasaki, Japan
- 2. The Hakubi Center for Advanced Research, Kyoto University, Kyoto, Japan
- 3. Atmosphere and Ocean Research Institute, The University of Tokyo, Chiba, Japan
- 4. Graduate School of Human and Environmental Studies, Kyoto University, Kyoto, Japan

*Corresponding author

Email: sakamoto.tatsuya.3p@kyoto-u.ac.jp

Present address: Yoshidanihonmatsucho, Kyoto Sakyo-ku, Kyoto, 606-8316 Japan

Supplementary Information

Comparison of sample preparation costs between eye lens and otolith processing Processing eye lenses require less equipment and time compared to otolith that has been traditionally used for similar purpose. For example, the preparation steps before isotope analysis for near-core area of an otolith include (1) resin embedding, (typically 3 h to cure), (2) grounding and polishing into section (0.5 h), (3) micromilling and powder collection (0.5 h) (Sakamoto et al., 2024). Micromilling system, for example Geomill 326 (Izumo-web) used for Japanese sardine, costs several ten thousand US dollars. On the contrary, eye lens central part of ~ 1mm diameter can be extracted in less than 10 mins under a stereomicroscope with scale (several thousand dollars).

Fish size-eye lens diameter relationship

The relationship between eye lens diameter and fish length was established to reconstruct fish size at the formation of a delaminated eye lens. Fish eye lenses have outer gelatinous cortex and inner hardened regions, and the inner part of the gelatinous cortex eventually

dehydrates to form the outer part of the hardened interior as the fish grows. The relationship between fish length and the diameter of dried whole eye lens is likely most suitable for reconstructing fish size, although drying eye lenses without considerable deformation are only possible for those from fresh fish, which are of limited availability. We therefore collected 137 fresh (113 to 220 mm in standard length (SL)) and 156 frozen sardine specimens (19 to 190 mm SL) from fisheries and supermarkets, and extracted the eye lenses. The diameter of whole wet lenses was measured when lens conditions allowed. Lenses from fresh samples were then air-dried in a refrigerator for several days, and the diameter of the solidified dried lenses were measured. For frozen and thawed samples, the gelatinous cortex region was removed and the diameter of the inner hardened region was measured. Assuming that the diameters have allometric relationships against fish standard length (*Eye lens diameter* $\sim a^*(SL)^b$) and that the ratio of the three diameters at a given fish length is consistent throughout growth (Leifsdóttir and Campana, 2023), we modelled the relationship between size and lens diameter using a linear random effect model as follows:

$$\ln(diameter) \sim a_i + b * \ln(SL) + (1|individual) \quad (i = 1,2,3)$$

$$\begin{cases} a_1: Wet \ whole \ lens \\ a_2: innter \ hardened \ region \\ a_3: Dried \ whole \ lens, \end{cases}$$

where (1|*individual*) represent the individual dependent random effect to account for the repeated measurements from the same individual. The *lmerTest* package (Kuznetsova et al., 2017) in R 4.1.3 (R Core Team, 2022) was used for the analysis.

The relationship between SL and three measures of eye lens diameter, namely the diameter of wet and whole lens (WW), dried and whole lens (DW), and the hardened inner area (HI) was modelled based on 402 measurements as follows:

$$\ln(Diameter) = \begin{cases} -3.64 \ (HI) \\ -3.28 \ (DW) + 0.879 * \ln(SL) + \sigma_{individual} + \sigma_{residual}, \\ -2.99 \ (DD) \end{cases}$$

where $\sigma_{individual}$ represent the standard deviation of individual random effect (0.06) and $\sigma_{residual}$ of the residual (0.10). Based on the relationship between fish size and DW diameter, which most closely represents the size at formation of delaminated, the eye lens centres of 0.7–1.0 mm diameter correspond to the portion formed from hatch to 28–42 mm SL.

Otolith stable isotope analysis protocol

Otoliths were embedded in epoxy resin (Petropoxy 154, Burnham Petrographics LLC), then polished along the sagittal plane until the core is revealed using sandpapers and alumina suspension (BAIKOWSKI International Corporation). The daily increments were examined along the axis in the postrostrum from the core as far as possible using an otolith measurement system (RATOC System Engineering Co. Ltd.). The otolith portions formed during 0-60 and 106-120 dph, representing the larval and juvenile stage respectively, were identified and milled out using a high-precision micro-milling system Geomill 326 (Izumo-web, Japan). The δ^{18} O and δ^{13} C of extracted powdered were analysed using an isotope ratio mass spectrometer (Delta V plus, Thermo Fisher Scientific) equipped with an automated carbonate reaction device (GasBench II, Thermo Fisher Scientific) at the Atmosphere and Ocean Research Institute, the University of Tokyo, Chiba (Shirai et al., 2018). The otolith powder (8 to 80 µg) was reacted with phosphoric acid at 72 °C. All isotope values are reported using delta notation relative to the Pee Dee Belemnite. Analytical precisions of δ^{18} O and δ^{13} C for international standards (NBS-19) were 0.06-0.13 (1σ) and 0.05-0.11 ‰, respectively. The commonly accepted acid fractionation factor of 1.01025 for calcite (Friedman and O'Neil, 1977) was used. Because the difference between the acid fractionation factor of calcite (standard material) and aragonite (otolith) depends on temperature (Kim et al., 2007), we subtracted 0.09 ‰ from the δ^{18} O value to allow comparison with data in previous studies analysed at 25 °C.

Supplementary Table 1. Data source of Japanese sardine catch.

Reference	Period
Ito, 1960	1917 to 1949
Ohshimo et al., 2009	1950 to 1959
FAO, 2024	1950 to 2022
Muko et al., 2023	1960 to 2022
Furuichi et al., 2023	1975 to 2022

Supplementary Table 2. Sample metadata.

11	,			1			
Region	Year	Month	Day	Latitude (°N)	Longitude (°E)	N	SL (mm, ±1SD)
East China Sea	2012	7	31	32.75	129.25	4	89.2 ± 6.2
East China Sea	2020	5	27	32.75	129.25	4	171.3 ± 12.0
East China Sea	2020	6	17	32.75	128.75	9	111.6 ± 8.6
East China Sea	2020	6	23	32.75	129.25	5	143.5 ± 5.8
East China Sea	2020	9	4	33.69	128.58	1	122.3
East China Sea	2020	11	5	32.71	128.88	11	147.2 ± 8.4
East China Sea	2020	11	5	31.93	129.9	13	141.9 ± 7.4
East China Sea	2020	11	11	31.93	129.9	10	130.4 ± 5.5
East China Sea	2020	11	18	31.93	129.9	15	145.1 ± 12.3
East China Sea	2020	12	3	32.75	129.25	17	151.0 ± 8.6
East China Sea	2021	2	12	32.75	129.25	2	211.6 ± 11.1
East China Sea	2021	2	24	32.75	129.25	2	162.0 ± 10.4
East China Sea	2021	4	17	32.75	129.25	10	164.8 ± 5.2
East China Sea	2021	4	30	32.75	129.25	9	175.3 ± 5.8
East China Sea	2021	10	30	32.55	129.96	8	144.5 ± 1.4
East China Sea	2022	9	26	32.3	130.01	12	118.3 ± 7.9
East China Sea	2023	3	11	31.98	130.01	19	185.8 ± 7.4
East China Sea	2023	3	15	32.53	129.5	16	191.8 ± 10.1
East China Sea	2023	3	16	32.75	129.25	19	187.6 ± 12.9
East China Sea	2023	3	22	32.75	129.25	20	206.4 ± 9.6
East China Sea	2023	4	21	31.98	130.01	20	193.4 ± 9.4
East China Sea	2023	5	12	31.98	130.01	19	191.9 ± 7.5
Sea of Japan	2013	6	14	36.79	137.17	7	29.1 ± 1.4
Sea of Japan	2017	8	10	36.25	133.08	12	94.9 ± 3.4
Sea of Japan	2017	8	18	36.25	133.08	10	95.7 ± 2.7
Sea of Japan	2017	8	28	36.25	133.08	9	97.7 ± 2.2
Sea of Japan	2017	9	8	35.75	133.08	12	105.1 ± 3.0
Sea of Japan	2017	12	9	37.75	133.2	1	146.8
Sea of Japan	2017	12	9	37.5	133.26	3	180.9 ± 34.7
Sea of Japan	2017	12	10	36.46	132.75	1	197.9
Sea of Japan	2018	8	31	37.32	135.98	13	122.7 ± 4.8
Sea of Japan	2018	9	2	34.65	130.57	7	111.6 ± 3.9
Sea of Japan	2019	4	4	36.79	137.08	17	166.9 ± 6.7
Sea of Japan	2019	4	25	36	135.55	12	143.8 ± 14.0
Sea of Japan	2019	8	24	37.86	135.6	16	106.3 ± 6.5
Sea of Japan	2020	3	4	35.75	133.25	10	181.2 ± 14.7
Sea of Japan	2020	3	19	35.75	133.25	4	173.8 ± 11.9
Sea of Japan	2020	4	3	35.75	133.08	10	180.8 ± 9.9
Sea of Japan	2020	4	8	36.79	137.08	8	180.6 ± 12.4
Sea of Japan	2020	4	10	37.25	137.15	10	190.3 ± 12.4
Sea of Japan	2020	4	15	36.34	134.5	1	151.7
Sea of Japan	2020	4	15	36.83	135.51	4	182.2 ± 14.8
Sea of Japan	2020	4	15	39.85	138.51	10	139.4 ± 16.4
Sea of Japan	2020	4	16	37.34	133.49	1	171.4
Sea of Japan	2020	4	16	36.86	133.49	6	191.7 ± 13.0
Sea of Japan	2020	4	16	35.83	135.51	3	187.7 ± 11.4
Sea of Japan	2020	4	17	37.84	133.49	3	189.4 ± 5.4
Sea of Japan	2020	4	18	38.84	134.49	1	156.6
Sea of Japan	2020	4	18	36.84	136.01	1	185.1
Sea of Japan	2020	6	24	40.37	139.67	8	170.0 ± 14.5
Sea of Japan	2020	6	30	41.02	138.33	2	184.1 ± 26.4
Sea of Japan	2020	7	3	38	137.88	12	186.6 ± 9.1
Sea of Japan	2020	7	7	44.09	139.97	1	188.1
Sea of Japan	2020	8	29	34.67	130.58	4	119.3 ± 2.1
Sea of Japan	2020	8	29	34.83	130.68	2	121.8 ± 0.7
Sea of Japan	2020	8	30	34.67	130.07	2	121.8 ± 4.9
Sea of Japan	2020	8	30	34.5	130.15	8	120.4 ± 5.9
Sea of Japan	2020	8	30	39.58	137.71	11	133.0 ± 16.3
Sea of Japan	2020	8	31	34.32	129.9	10	117.4 ± 3.0

Supplementary Table 2. Continued.

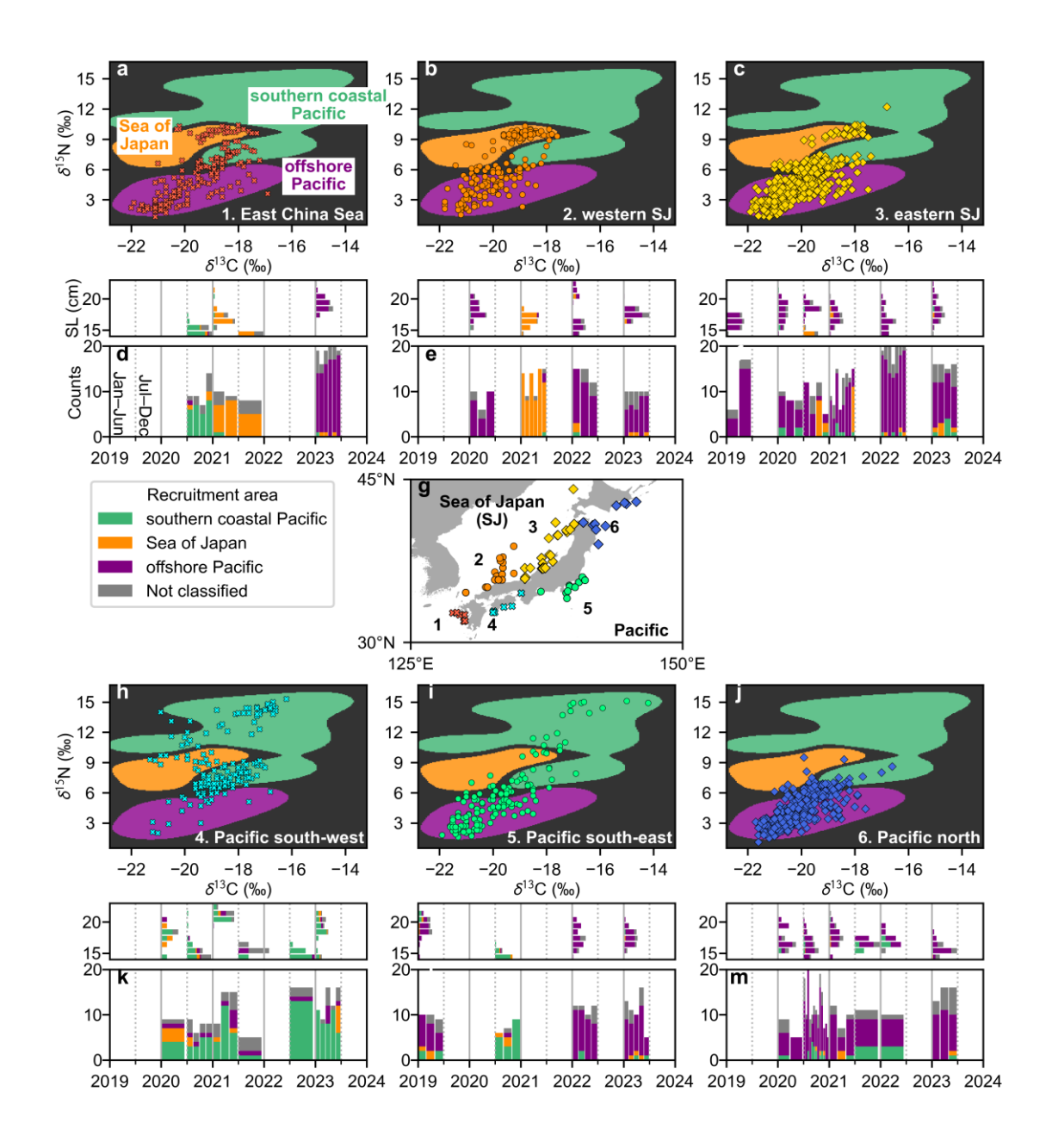
Region	Year	Month	Day	Latitude (°N)	Longitude (°E)	N	SL (mm, ±1SD)
Sea of Japan	2020	9	3	38.07	137.76	10	121.0 ± 29.0
Sea of Japan	2020	9	4	37.44	138.07	9	191.7 ± 5.7
Sea of Japan	2020	9	6	39.85	138.55	20	142.6 ± 10.6
Sea of Japan	2020	9	7	40.3	139.31	14	$148.6~\pm~26.5$
Sea of Japan	2020	9	7	40.12	139.39	10	$132.7~\pm~8.9$
Sea of Japan	2020	9	12	37.33	134.17	1	129.2
Sea of Japan	2020	9	14	35.83	134.17	4	121.5 ± 3.1
Sea of Japan	2020	9	17	36.29	133.43	1	120.3
Sea of Japan	2020	10	27	35.75	133.25	10	129.5 ± 3.2
Sea of Japan	2021	1	5	36.79	137.17	13	120.1 ± 9.4
Sea of Japan	2021	2	14	40.88	140.04	9	187.7 ± 12.2
Sea of Japan	2021	3	7	40.88	140.04	7	176.1 ± 14.5
Sea of Japan	2021	3	8	35.08	132.08	9	151.6 ± 6.0
Sea of Japan	2021	3	8	36.79	137.08	15	170.5 ± 17.2
Sea of Japan	2021	3	12	35.75	133.42	14	164.2 ± 5.1
Sea of Japan	2021	4	9	36.79	137.17	14	169.1 ± 15.7
Sea of Japan	2021	4	11	40.88	140.04	6	172.8 ± 15.4
Sea of Japan	2021	4	14	35.86	135.51	3	179.9 ± 16.7
Sea of Japan	2021	4	16	35.75	132.75	14	160.0 ± 4.1
Sea of Japan	2021	4	28	35.75	133.08	4	$33.3~\pm~3.3$
Sea of Japan	2021	4	28	37.76	137.04	13	171.2 ± 9.6
Sea of Japan	2021	5	12	36.79	137.17	13	171.1 ± 12.7
Sea of Japan	2021	5	14	35.75	133.08	6	36.2 ± 1.7
Sea of Japan	2021	6	1	35.08	131.92	9	167.6 ± 5.1
Sea of Japan	2021	6	2	35.75	133.08	1	28.5
Sea of Japan	2021	6	3	36.25	133.42	15	173.2 ± 2.1
Sea of Japan	2021	6	11	35.51	133.34	3	27.6 ± 2.6
Sea of Japan	2021	6	15	36.08	132.92	15	178.2 ± 5.6
Sea of Japan	2021	6	29	36.79	137.08	15	178.9 ± 6.0
Sea of Japan	2021	7	13	39.58	138.74	15	85.8 ± 5.3
Sea of Japan	2021	7	13	39.58	138.75	15	85.6 ± 4.5
Sea of Japan	2021	7	13	39.59	138.76	13	86.1 ± 4.0
Sea of Japan	2021	7	14	39.28	137.95	12	82.7 ± 4.7
Sea of Japan	2021	7	14	39.28	137.96	14	81.4 ± 4.0
Sea of Japan	2021	7	14	39.26	137.96	14	82.5 ± 4.1
Sea of Japan	2021	7	15	38.52	137.49	1	90.6
Sea of Japan	2021	7	16	35.75	133.08	14	103.8 ± 6.3
Sea of Japan	2021	7	21	35.75	133.08	1	64.8
Sea of Japan	2021	9	14	36.79	137.08	7	87.8 ± 5.0
Sea of Japan	2022	1	25	40.88	140.04	19	182.1 ± 21.0
Sea of Japan	2022	2	15	36.79	137.08	20	163.2 ± 12.9
Sea of Japan	2022	2	15	36.79	137.17	20	163.2 ± 12.9
Sea of Japan	2022	2	15	40.88	140.04	16	175.4 ± 21.6
Sea of Japan	2022	2	17	37.27	137.16	20	170.7 ± 17.5
Sea of Japan	2022	3	4	35.75	133.08	15	156.8 ± 5.2
Sea of Japan	2022	3	8	35.75	133.08	15	145.9 ± 19.4
Sea of Japan	2022	3	23	34.58	130.08	15	208.7 ± 12.2
Sea of Japan	2022	3	29	36.84	137.36	20	175.0 ± 9.2
Sea of Japan	2022	3	29	36.84	137.39	20	151.4 ± 6.7
Sea of Japan	2023	2	7	36.79	137.17	15	189.4 ± 12.2
Sea of Japan	2023		10	36.84	137.36	16	194.0 ± 23.0
Sea of Japan	2023		20	36.89	137.2	16	166.7 ± 10.3
Sea of Japan	2023		24	35.75	133.08	10	175.3 ± 5.1
Sea of Japan	2023		14	35.75	133.08	10	172.1 ± 6.0
Sea of Japan	2023		16	36.79	137.17	16	177.8 ± 9.4
Sea of Japan	2023		5	35.75	133.08	10	179.5 ± 4.4
Sea of Japan	2023		14	35.75	133.08	10	182.4 ± 9.7
Sea of Japan	2023		9	35.75	133.08	10	174.5 ± 5.8
1		-				-	

Supplementary Table 2. Continued.

Region	Year	Month	Day	Latitude (°N)	Longitude (°E)	N	SL (mm, ±1SD)
southern coastal Pacific	2019	3	18	35.53	140.48	10	197.1 ± 11.4
southern coastal Pacific	2019	3	27	34.54	139.3	10	189.8 ± 9.7
southern coastal Pacific	2019	4	22	35.53	140.48	9	$191~\pm~24.2$
southern coastal Pacific	2019	9	17	35.23	139.59	8	122.2 ± 16.5
southern coastal Pacific	2020	2	20	32.88	132.63	9	179.8 ± 16.9
southern coastal Pacific	2020	7	6	34.53	135.18	6	125.1 ± 3.3
southern coastal Pacific	2020	10	1	34.53	135.18	8	126.2 ± 10.9
southern coastal Pacific	2020	10	9	34.18	136.53	10	129.9 ± 3.7
southern coastal Pacific	2020	10	15	34.67	136.98	10	140.1 ± 4.6
southern coastal Pacific	2020	10	24	35.53	140.48	10	126.3 ± 2.4
southern coastal Pacific	2020	10	26	34.67	136.98	10	$128.2~\pm~5.5$
southern coastal Pacific	2020	10	26	35.23	139.59	15	134.4 ± 7.3
southern coastal Pacific	2020	10	27	32.75	132.58	16	143.1 ± 12.3
southern coastal Pacific	2020	10	28	35.53	140.48	12	139.7 ± 11.0
southern coastal Pacific	2020	11	5	33.33	134.33	10	123.6 ± 5.9
southern coastal Pacific	2020	11	6	32.75	132.58	15	144.5 ± 15.1
southern coastal Pacific	2020	11	12	32.75	132.58	15	137.8 ± 10.8
southern coastal Pacific	2020	11	14	34.18	136.53	9	130 ± 2.6
southern coastal Pacific	2020	11	20	35.23	139.59	8	128.2 ± 4.6
southern coastal Pacific	2020	11	25	32.75	132.58	13	147.9 ± 15.3
southern coastal Pacific	2020	12	1	33.33	134.33	9	129.3 ± 9.2
southern coastal Pacific	2020	12	5	32.88	132.63	10	123.8 ± 6.6
southern coastal Pacific	2020	12	5	35.14	139.62	13	146.1 ± 9.9
southern coastal Pacific	2020	12	23	32.75	132.75	3	192 ± 24.8
southern coastal Pacific	2021	1	5	32.75	132.58	15	208.3 ± 6.5
southern coastal Pacific	2021	1	20	33.25	133.58	8	215.7 ± 6.9
southern coastal Pacific	2021	2	4	33.25	133.58	15	214.7 ± 7.1
southern coastal Pacific	2021	7	13	34.53	135.18	8	118.3 ± 6.0
southern coastal Pacific	2021	8	6	34.67	136.98	2	118.4 ± 2.8
southern coastal Pacific	2021	9	11	34.53	135.18	7	126.3 ± 2.2
southern coastal Pacific	2021	11	12	33.33	134.33	5	153.9 ± 4.3
southern coastal Pacific	2022	1	24	35.83	140.93	12	183.4 ± 17.1
southern coastal Pacific	2022	2	3	35.33	140.47	9	121.6 ± 2.8
southern coastal Pacific	2022	2	9	35.71	141.04	20	150.8 ± 27.9
southern coastal Pacific	2022	2	14	35.07	140.13	12	169.1 ± 15.0
southern coastal Pacific	2022	3	22	34.05	139.38	12	180.9 ± 10.5
southern coastal Pacific	2022	3	31	32.75	132.58	3	102 ± 11.8
southern coastal Pacific	2022	5	13	33.42	133.42	12	86 ± 5.2
southern coastal Pacific	2022	5	20	32.75	132.58	16	113 ± 8.2
southern coastal Pacific	2022	8	9	32.75	132.58	16	149.3 ± 5.6
southern coastal Pacific	2023	1	18	34.53	135.18	11	179.7 ± 4.5
southern coastal Pacific	2023	1	27	32.75	132.58	4	169.4 ± 23.9
southern coastal Pacific	2023	2	4	34.71	139.45	5	180.8 ± 7.2
southern coastal Pacific	2023	2	17	34.53	135.18	10	$145~\pm~4.3$
southern coastal Pacific	2023	2	17	36	140.8	13	172.6 ± 14.6
southern coastal Pacific	2023	2	22	34.71	139.45	11	177.3 ± 11.3
southern coastal Pacific	2023	2	24	36	140.8	10	175.6 ± 12.4
southern coastal Pacific	2023	2	28	36	140.8	16	180.1 ± 11.5
southern coastal Pacific	2023	3	17	32.75	132.58	16	201.2 ± 4.4
southern coastal Pacific	2023	3	18	34.53	135.18	12	186.7 ± 5.1
southern coastal Pacific	2023	5	17	32.75	132.58	16	212.1 ± 6.8
remain constant natific	2023	5	1,	32.13	132.30	10	2.2 ± 0.0

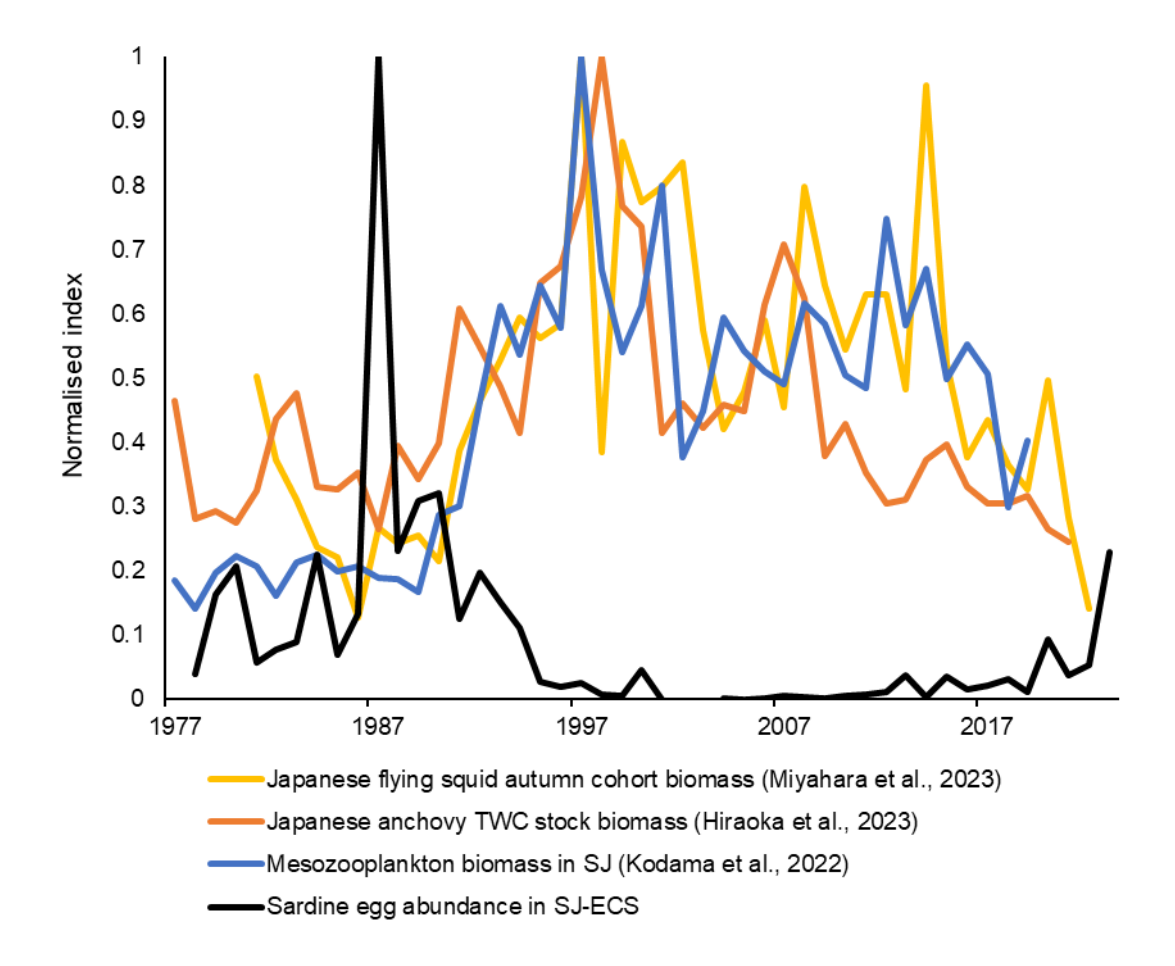
Supplementary Table 2. Continued.

Region	Year	Month	Day	Latitude (°N)	Longitude (°E)	N	SL (mm, ±1SD)
northern coastal Pacific	2020	4	2	41.02	140.88	9	164.4 ± 7.9
northern coastal Pacific	2020	5	11	41.02	140.88	10	156.5 ± 33.9
northern coastal Pacific	2020	7	2	41.02	140.88	12	159.8 ± 21.9
northern coastal Pacific	2020	7	5	39.02	142.27	10	155.8 ± 8.3
northern coastal Pacific	2020	7	9	40.7	142.92	10	$157.0~\pm~7.3$
northern coastal Pacific	2020	7	20	42.57	143.92	18	164.0 ± 15.9
northern coastal Pacific	2020	7	26	42.93	145.75	26	170.4 ± 14.6
northern coastal Pacific	2020	8	3	41.02	140.88	16	156.9 ± 15.8
northern coastal Pacific	2020	8	19	40.78	141.75	12	$172.0~\pm~13.5$
northern coastal Pacific	2020	9	4	41.02	140.88	10	$162.0~\pm~9.3$
northern coastal Pacific	2020	9	8	42.83	144.67	19	162.8 ± 11.6
northern coastal Pacific	2020	9	22	42.47	145.84	13	119.6 ± 3.8
northern coastal Pacific	2020	10	1	42.73	144.85	16	160.9 ± 13.7
northern coastal Pacific	2020	11	16	41.02	140.88	18	124.0 ± 26.2
northern coastal Pacific	2020	12	10	40.36	142.05	8	183.9 ± 21.6
northern coastal Pacific	2020	12	23	41.02	140.88	6	$144.4~\pm~5.4$
northern coastal Pacific	2020	12	23	40.36	142.05	4	180.2 ± 15.7
northern coastal Pacific	2021	3	17	41.02	140.88	12	178.9 ± 22.1
northern coastal Pacific	2021	4	13	41.02	140.88	15	150.3 ± 24.5
northern coastal Pacific	2021	5	26	41.02	140.88	10	181.8 ± 10.7
northern coastal Pacific	2021	8	2	40.88	141.95	12	160.3 ± 11.8
northern coastal Pacific	2021	9	26	42.62	144.53	7	$112.7~\pm~6.6$
northern coastal Pacific	2022	1	18	41.02	140.88	10	110.3 ± 10.8
northern coastal Pacific	2022	3	2	41.02	140.88	20	125.5 ± 50.2
northern coastal Pacific	2023	4	19	41.02	140.88	16	152.8 ± 10.8
northern coastal Pacific	2023	5	15	41.02	140.88	16	162.6 ± 9.3
northern coastal Pacific	2023	6	6	41.02	140.88	16	156.3 ± 10.2
offshore Pacific	2015	9	18	43.91	155.14	12	$125.3~\pm~3.6$
offshore Pacific	2015	9	18	44.68	156.38	14	$126.6~\pm~8.4$
offshore Pacific	2019	8	24	44.5	175.15	2	$120.8~\pm~4.9$
offshore Pacific	2019	9	15	45.2	158.52	9	$128.1~\pm~2.9$
offshore Pacific	2020	9	28	46.25	174.84	19	151.0 ± 10.1
offshore Pacific	2020	10	4	46.09	159.99	17	$135.6~\pm~8.4$
offshore Pacific	2020	10	4	46.44	160.52	17	$141.0~\pm~10.6$
offshore Pacific	2021	5	18	38.44	147.02	2	$35.6~\pm~0.1$
offshore Pacific	2021	5	18	38.44	147.02	2	$33.9~\pm~0.8$
offshore Pacific	2021	5	18	38.33	147.11	3	$35.8~\pm~1.4$
offshore Pacific	2021	5	18	37.69	148.42	1	35.1
offshore Pacific	2021	5	19	37.51	149.32	4	$37.6~\pm~3.4$
offshore Pacific	2021	5	29	38.34	146.5	7	$68.6~\pm~3.5$
offshore Pacific	2021	5	30	38.92	150.15	7	$67.7 ~\pm~ 3.2$
offshore Pacific	2021	5	31	38.3	153.33	7	$80.6~\pm~7.0$
offshore Pacific	2021	6	26	40.16	178.97	9	$109.6~\pm~6.4$
offshore Pacific	2021	9	23	44.69	161.46	1	121.3
offshore Pacific	2021	9	29	48.28	175.13	6	$125.2~\pm~3.5$



Supplementary Figure 1. Population-wide mixing from different recruitment

sources. The δ^{13} C and δ^{15} N values of eye lens centres of adults from the East China Sea (a), western Sea of Japan (b) and eastern Sea of Japan (c), overlaid on classification model background colours (Figure 2g, h). Counts of fish from three nursery areas and unclassified individuals in each region (d–f), with each bar representing a sampling batch (6–20 individuals), sorted by date and grouped into half-year blocks (d–f). Length frequency for each block is shown above (d–f). Sampling locations of adults (g). Isotope values of fish from the western (h) and eastern (i) part of the southern coastal Pacific, and the northern coastal Pacific (j), and the temporal variation of the proportion (k–m).



Supplementary Figure 2. Timeseries of zooplankton and major zooplankton feeders in the SJ-ECS. All the indices are scaled between 0 and 1. Note that the biomass of Japanese sardine is proxied by survey-based egg abundance (Seikai National Fisheries Research Institute, 2003; Muko et al., 2024) instead of estimated biomass in stock-assessments as the assessment model includes significant uncertainty in the assumed population structure.

References

- FAO, Fishery and Aquaculture Statistics 2023. FAO Yearbook (2023).
- Friedman, I. and O'Neil, J.R. Compilation of Stable Isotope Fractionation Factors of Geochemical Interest. U.S. Geol. Surv. Professional Paper 440-KK, Data of Geochemistry, 6th Edition, Chapter KK, KK1–KK12 (1977).
- Furuichi, S. et al. Stock assessment and evaluation for the Pacific stock of Japanese sardine (fiscal year 2023). In Marine fisheries subpopulation assessment and evaluation for Japanese waters. Japan Fisheries Agency and Japan Fisheries Research and Education Agency, Tokyo, 52pp (2024). https://abchan.fra.go.jp/wpt/wp-content/uploads/2024/03/details_2023_01.pdf
- Hiraoka, Y. et al. Stock assessment and evaluation for the Tsushima Warm Current subpopulation of Japanese anchovy (fiscal year 2023). In Marine fisheries subpopulation assessment and evaluation for Japanese waters. Japan Fisheries Agency and Japan Fisheries Research and Education Agency, Tokyo, 50pp (2024). https://abchan.fra.go.jp/wpt/wp-content/uploads/2024/03/details_2023_26.pdf
- Ito, S. Fishery biology of the Japanese sardine, *Sardinops melanosticta* (T. & S.), in the waters around Japan. Bull. Japan Sea Reg. Fish. Res. Lab. 9, 1-227 (1961).
- Kim, S., Mucci, A. & Taylor, B. E. Phosphoric acid fractionation factors for calcite and aragonite between 25 and 75 °C: revisited. Chem. Geol. 246, 135–146 (2007).
- Kodama, T., Igeta, Y. & Iguchi, N. Long-Term Variation in Mesozooplankton Biomass Caused by Top-Down Effects: A Case Study in the Coastal Sea of Japan. Geophys. Res. Lett. 49, e2022GL099037 (2022).
- Kuznetsova, A., Brockhoff, P. B. & Christensen, R. H. ImerTest package: tests in linear mixed effects models. J. Stat. Softw. 82, 1–26 (2017).
- Miyahara, T. et al. Stock assessment and evaluation for the autumn cohort of Japanese flying squid (fiscal year 2023). In Marine fisheries subpopulation assessment and evaluation for Japanese waters. Japan Fisheries Agency and Japan Fisheries Research and Education Agency, Tokyo, 87pp (2024). https://abchan.fra.go.jp/wpt/wpcontent/uploads/2024/03/details_2023_19.pdf
- Muko, S. et al. Stock assessment and evaluation for the Tsushima Warm Current subpopulation of Japanese sardine (fiscal year 2023). In Marine fisheries subpopulation assessment and evaluation for Japanese waters. Japan Fisheries Agency and Japan Fisheries Research and Education Agency, Tokyo, 61pp (2024). https://abchan.fra.go.jp/wpt/wp-content/uploads/2024/03/details_2023_02.pdf
- Ohshimo, S., Tanaka, H. & Hiyama, Y. Long-term stock assessment and growth changes

- of the Japanese sardine (*Sardinops melanostictus*) in the Sea of Japan and East China Sea from 1953 to 2006. Fish. Oceanogr. 18, 346–358 (2009).
- Sakamoto, T., Takahashi, M., Shirai, K., Aono, T. & Ishimura, T. Fisheries shocks provide an opportunity to reveal multiple recruitment sources of sardine in the Sea of Japan. Sci. Rep. 14, 21722 (2024).
- Seikai National Fisheries Research Institute. Current status of small pelagic fish in the East China Sea and Sea of Japan, the mechanism of stock fluctuations of Japanese sardine, anchovy and round herring. Fisheries Research Agency of Japan, Yokohama, 23pp (2003). https://abchan.fra.go.jp/pr/maiwashi0404/maiwashi0404.pdf
- Shirai, K. *et al.* Reconstruction of the salinity history associated with movements of mangrove fishes using otolith oxygen isotopic analysis. *Mar. Ecol. Prog. Ser.* **593**, 127–139 (2018).